

Data-driven confidence bound for structural response using segmented least squares: a mixed-integer programming approach

Yoshihiro Kanno

Received: date / Accepted: date

Abstract As one of data-driven approaches to computational mechanics in elasticity, this paper presents a method finding a bound for structural response, taking uncertainty in a material data set into account. For construction of an uncertainty set, we adopt the segmented least squares so that a data set that is not fitted well by the linear regression model can be dealt with. Since the obtained uncertainty set is nonconvex, the optimization problem solved for the uncertainty analysis is nonconvex. We recast this optimization problem as a mixed-integer programming problem to find a global optimal solution. This global optimality, together with a fundamental property of the order statistics, guarantees that the obtained bound for the structural response is conservative, in the sense that, at least a specified confidence level, probability that the structural response is in this bound is no smaller than a specified target value. We present numerical examples for three different types of skeletal structures.

Keywords Data-driven computing · Mixed-integer programming · Global optimization · Order statistics · Reliability with unknown distribution

Mathematics Subject Classification (2020) 90C11 · 62G30 · 90C57 · 90B25

1 Introduction

Conventional computational mechanics assumes a model of the constitutive law specific to a material. For example, in the static equilibrium analysis of elastic solids and structures, the constitutive law relates the stress to the strain. It is usual that the constitutive law is determined through empirical modeling of the stress–strain relation, followed by calibration of the parameters in the model. In contrast, data-driven approaches to computational mechanics have recently attracted substantial attention,

Yoshihiro Kanno

Corresponding author. Address: Mathematics and Informatics Center, The University of Tokyo, Hongo 7-3-1, Tokyo 113-8656, Japan. E-mail: kanno@mi.st.i.u-tokyo.ac.jp.

where a material data set is utilized directly for the structural analysis, without resorting to the conventional process of modeling and calibration.

The contribution that activates emerging study of data-driven methods in computational mechanics is Kirchdoerfer and Ortiz [29], where, provided that a data set of material experiments (i.e., a set of pairs of observed stress and strain values) is given, the structural response at the static equilibrium state is estimated. Specifically, based on the conventional finite element method, the stress and strain at each integration point are considered unknowns subjected to the compatibility condition and the force-balance equation. Then the pair of stress and strain values that has the minimum distance, in some sense, to the data set is declared as the equilibrium state. Kirchdoerfer and Ortiz [29] defined the distance from a point in the stress–strain space to a data set as the Euclidean distance (with a scaling) from the point to the closest data point. This methodology is sometimes called the *distance-minimizing method* [36, 37], and has rapidly been applied to diverse problem settings, including elasticity with geometrical nonlinearity [35], history-dependent elastoplastic problems [2, 5, 6, 37, 38], brittle fracture [1], and diffusion problems [36]. It has also been extended to multi-scale modelings of, e.g., composites [49], bone tissue [34], and granular materials [28]. Moreover, instead of a data set of material experiments, usage of a data set of structural experiments has also been studied [4, 31, 40]. It is worth noting that, for the multi-scale modeling [28], etc., a material data set is sometimes generated by using numerical simulation. This is analogous to preparation of a data set by numerical material tests using the computational homogenization method to identify the macroscopic material properties of composites and polycrystalline metals with periodic micro-structures [3, 45, 46, 48].

An alternative methodology of data-driven computational mechanics adopts the notion of so-called *constitutive manifold*. Namely, the points satisfying the constitutive law usually do not exist ubiquitously in whole of the stress–strain space, but lie on a manifold with a lower dimension than the space. Ibañez *et al.* [14, 15] proposed to use a locally linear embedding, which is one of popular methods for the manifold learning, to capture the constitutive manifold. He and Chen [11], He *et al.* [12], and Su *et al.* [41] proposed methods that construct a local convex envelop from the neighboring data points. The author proposed kernel-based methods for extracting the constitutive manifold [25, 26].

Other approaches to data-driven computational mechanics are also found in literature. Luo and Paal [32] proposed a variant of the support vector regression that is robust against presence of outliers, and applied it to the static equilibrium analysis of an elastic truss. Tang *et al.* [42, 43, 44] developed a method recovering the three-dimensional stress–strain relation from material data of the uniaxial experiments. This method was applied to continuum-based topology optimization in conjunction with the moving morphable void method [9]. Prume *et al.* [39] supposed that the material response is random. A certain likelihood is given for each data point of a material data set, and the distribution of material response is estimated by minimizing the Kullback–Leibler divergence. Accordingly, Prume *et al.* [39] evaluated the expected value of the structural response.

Motivated by the observation that, in the presence of even a single outlier, the method proposed by Kirchdoerfer and Ortiz [29] can possibly converge to a very

improper solution (see [22, Remark 2] and [8, Remark 1]), Guo *et al.* [8] proposed a distinctive method that introduces the concept of worst-case analysis under non-probabilistic uncertainty [24] to the data-driven computational mechanics. Specifically, when a set of pairs of stress and strain values is given, this method considers an ellipsoid including all the data points as the uncertainty set. A bound of the structural response is then obtained by solving an optimization problem under the constraints that each pair of the element stresses and strains belongs to the ellipsoid, together with the compatibility condition and the force-balance equation. It is worth noting that this optimization problem is convex, and hence can be solved globally, which guarantees the conservativeness of the obtained response bound. Thus, the distinguished feature of the method of Guo *et al.* [8] is that it provides upper and lower bounds, rather than a single value, of the quantity of interest. This is attractive from the perspective of the *uncertainty quantification* (UQ) [7], because the aleatory uncertainty, a.k.a. the natural variability, inevitably and intrinsically exists in material properties.

Inspired by Guo *et al.* [8], Kanno [27] proposed a method finding a response bound with a specified confidence. More precisely, it is guaranteed that, at least a specified confidence level, the probability that the structural response belongs to the obtained bound is no smaller than the target reliability. Here, the material property is not considered deterministic but stochastic, and given material data are supposed to be independent and identically distributed samples drawn from a distribution. A key is that the number of data points which the uncertainty set should include to guarantee the specified confidence level can be given by a fundamental property of the order statistics. Accordingly, the method does not require any modeling of the distribution, and hence is viewed as a model-free and data-driven UQ method. It is worth noting that the notion of confidence level is borrowed from studies on the reliability-based design optimization under uncertainty in the input distribution [10, 17, 18, 19, 21, 23, 33, 47].

A drawback of Kanno [27] is that, as it uses the linear regression to construct the uncertainty set, its applicability is limited to approximately linear material data: For a nonlinear elastic material, the bound obtained by this method can drastically overestimate the structural response. Use of the linear regression is motivated by the desire to guarantee the global optimality of solutions of the optimization problems for finding the response bound; a local optimal solution in general underestimates the structural response. In fact, the method of Guo *et al.* [8] has the same drawback, where it solves an optimization of linear objective function under convex quadratic constraints, while the method of Kanno [27] solves a linear programming problem. To deal with this drawback, Huang *et al.* [13] proposed to use a local uncertainty set for each element stress and strain, rather than a unique global ellipsoid that is common to all the elements. Specifically, this method adopts the convex hull of data points only in the neighborhood of each incumbent element stress and strain point. As a result, the method lacks guarantee of the global optimality, and hence the obtained solution in general underestimates the structural response. In contrast, this study attempts to deal with the drawback mentioned above with maintaining guarantee of the global optimality. Specifically, we extend the method of Kanno [27] by adopting the segmented least squares, instead of the linear regression. Although the induced uncertainty set is nonconvex, we show that this set is handled within the framework of

mixed-integer linear programming (MILP), which is a key to guaranteeing the global optimality.

One of potential advantages of the proposed method, as well as other methods based on uncertainty analysis [8, 13, 27], over the distance-minimizing methods [1, 2, 4, 5, 6, 28, 29, 31, 34, 35, 36, 37, 38, 40, 49] is that it does not require a large number of data points. For example, in the numerical experiments, Kirchdoerfer and Ortiz [29, section 3], Nguyen and Keip [35, section 4.2], and Poelstra *et al.* [38, section 5.3] used data sets consisting of about 10^6 data points; Nguyen *et al.* [36, section 2.8.2] used up to about 1.6×10^5 data points; and He and Chen [11, section 5] used up to about 5.1×10^5 data points. In contrast, the methods proposed in [27] and this paper can be applied even when the number of data points is relatively small (as demonstrated in section 6), where the upper bounds for the confidence level and target reliability become small. Precisely, by putting $\tilde{p} = r$ in (3) in section 2, we see that for the specified target reliability $1 - \epsilon \in]0, 1[$ the upper bound for the realizable confidence level is $1 - \delta = 1 - (1 - \epsilon)^r$, where r is the number of data points. For example, if the data set has $r = 500$ data points and we choose $\epsilon = 0.01$, then the minimum value of δ is about $6.57 \times 10^{-3} \simeq (1 - \epsilon)^r$.

The remaining paper is organized as follows: Section 2 revisits the framework proposed in [27] to introduce some useful definitions, and clarifies contributions of this study. Section 3 presents a *mixed-integer programming* (MIP) formulation for the segmented least squares, which is used to construct an uncertainty set in the stress–strain space. Section 4 shows that we can express the uncertainty set as some linear inequalities with some 0-1 variables, which enables us to formulate the optimization problem for finding a bound for the quantity of interest as a MIP problem. For simplicity, a concrete MIP formulation for finding a bound for the structural response is presented only for trusses in section 5. In section 6, we perform numerical experiments on three types of skeletal structures. Section 7 presents the conclusions.

2 Framework of computation with confidence

For completeness and ease of comprehension, we first overview the framework of the method proposed in the previous work [27]. We next identify the aims and contributions of this study.

2.1 Confidence bound for structural response

Suppose that we attempt to find a bound for the static response of an elastic structure. Assume that the quantity of interest, denoted by q , depends on a random vector $\mathbf{z} \in \mathbb{R}^c$, where c is the number of random variables. As a forecast of the structural response, consider a bound such that the probability that the realization of $q(\mathbf{z})$ is not included in this bound is no greater than the specified value, $\epsilon \in]0, 1[$, where $1 - \epsilon$ is called the *target reliability*. Note that, in this paper, we use $]a, b[$ and $[a, b]$ to denote the open interval and closed interval, respectively, between $a \in \mathbb{R}$ and $b \in \mathbb{R}$. If we know the

joint distribution function, F , of \mathbf{z} , then we seek to find $q \in \mathbb{R}$ and $\bar{q} \in \mathbb{R}$, i.e., lower and upper bounds for the quantity of interest, respectively, satisfying

$$\mathbb{P}\{q(\mathbf{z}) \in [q, \bar{q}]\} \geq 1 - \epsilon. \quad (1)$$

In reality, we have no knowledge on F . Instead, suppose that we are given a data set of \mathbf{z} , which consists of a finite number of continuous independent and identically distributed samples, denoted by $\check{z}_1, \dots, \check{z}_r \in \mathbb{R}^c$, drawn from F . We consider a lower bound constraint for the probability that constraint (1) is satisfied, i.e.,

$$\mathbb{P}_F\{\mathbb{P}\{q(\mathbf{z}) \in [q, \bar{q}]\} \geq 1 - \epsilon\} \geq 1 - \delta, \quad (2)$$

where $\delta \in]0, 1[$ is a specified value, $1 - \delta$ is called the *target confidence level*, and $\mathbb{P}_F\{\cdot\}$ means the probability taken for all possible F for which $\check{z}_1, \dots, \check{z}_r$ are continuous independent and identically distributed samples.

The data-driven concept in [27] is based on the order statistics, and does not resort to any empirical modeling of F . Let \tilde{p} denote the minimum integer satisfying

$$\sum_{k=\tilde{p}}^r \binom{r}{k} (1 - \epsilon)^k \epsilon^{r-k} \leq \delta. \quad (3)$$

We use $Z \subset \mathbb{R}^c$ to denote a set containing \tilde{p} samples among given samples $\check{z}_1, \dots, \check{z}_r$. It follows from Theorem 2.1 and the discussion in section 3 in Kanno [27] that Z satisfies

$$\mathbb{P}_F\{\mathbb{P}\{\mathbf{z} \in Z\} \geq 1 - \epsilon\} \geq 1 - \delta.$$

Accordingly, we see that q and \bar{q} defined by

$$q = \min\{q(\mathbf{z}) \mid \mathbf{z} \in Z\}, \quad (4)$$

$$\bar{q} = \max\{q(\mathbf{z}) \mid \mathbf{z} \in Z\} \quad (5)$$

satisfy (2).

2.2 Contributions of this study

As a concrete example consider a truss, where the constitutive law relates the uniaxial stress $\sigma \in \mathbb{R}$ to the uniaxial strain $\varepsilon \in \mathbb{R}$. We use $\sigma_e \in \mathbb{R}$ and $\varepsilon_e \in \mathbb{R}$ to denote the stress and strain of member e ($e = 1, \dots, m$), respectively, where m is the number of members of the truss.

Suppose that the constitutive law essentially has uncertainty. We are given a set of continuous independent and identically distributed samples, denoted by $D = \{(\check{\varepsilon}_1, \check{\sigma}_1), \dots, (\check{\varepsilon}_r, \check{\sigma}_r)\}$, drawn from the probability distribution that (ε, σ) follows. We use $C(\tau) \subset \mathbb{R}^2$ to denote the uncertainty set of (ε, σ) , where $\tau > 0$ is a parameter representing the magnitude of uncertainty. In [27], we adopted a set depicted in Figure 1a as $C(\tau)$, i.e.,

$$C(\tau) = \{(\varepsilon, \sigma) \in \mathbb{R} \times \mathbb{R} \mid |\alpha\varepsilon + \beta\sigma - \gamma| \leq \tau\}, \quad (6)$$

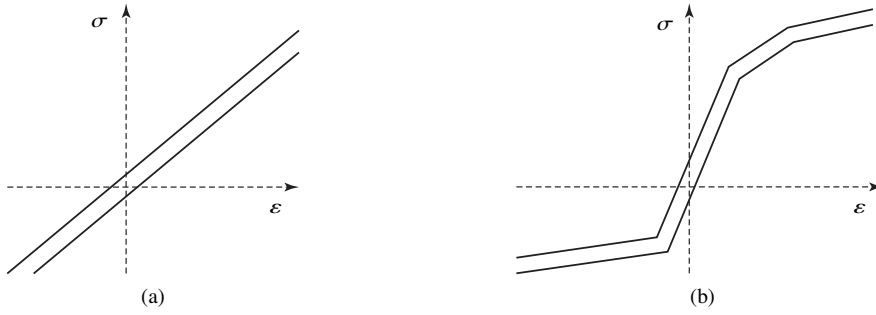


Fig. 1: Uncertainty set $C(\tau)$ of (ε, σ) . (a) The one considered in [27]; and (b) an example handled in this study.

where $\alpha, \beta, \gamma \in \mathbb{R}$ are constants. We set the value of τ so that $C(\tau)$ includes \tilde{p} samples among $(\check{\varepsilon}_1, \check{\sigma}_1), \dots, (\check{\varepsilon}_r, \check{\sigma}_r)$. Then, from the discussion in section 2.1 we obtain

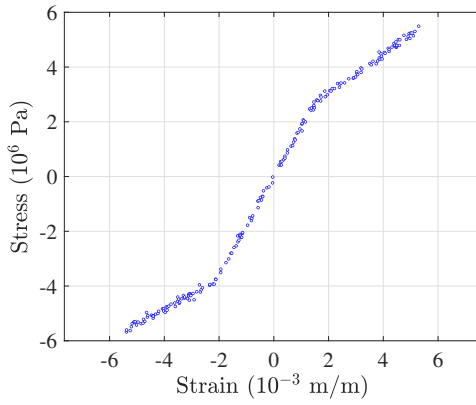
$$P_F\{P\{(\varepsilon, \sigma) \in C(\tau)\} \geq 1 - \epsilon\} \geq 1 - \delta.$$

Accordingly, we can formulate an optimization problem corresponding to problem (4) as follows: The optimization variables are the nodal displacements, member stresses, and member strains. The constraints are (i) the compatibility relations between the nodal displacements and the member strains, (ii) the force-balance equations in terms of the member stresses and the nodal external forces, and (iii) the inclusions

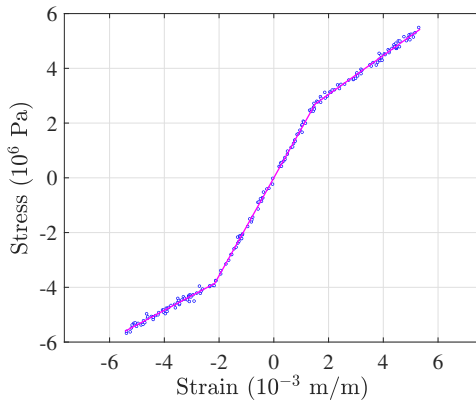
$$(\varepsilon_e, \sigma_e) \in C(\tau), \quad e = 1, \dots, m.$$

With this setting we minimize the quantity of interest to obtain its lower bound q satisfying (2). Also, an upper bound \bar{q} satisfying (2) is obtained by maximizing the quantity of interest [27].

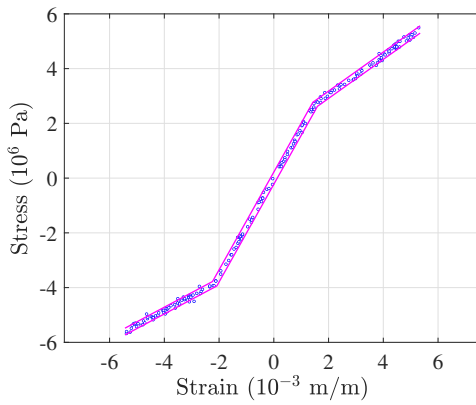
The aim of this study is to develop a method that can adopt a set depicted in Figure 1b as $C(\tau)$. Suppose that the data set shown in Figure 2a is given as a set of samples of (ε, σ) . If we adopt the set shown in Figure 1a as $C(\tau)$, then the solution obtained by the method in [27] becomes too conservative, i.e., the solution extremely overestimates the structural response. In such a case the set shown in Figure 1b mitigates overestimate drastically, which is exactly the motivation of this study. The key is that this paper presents a method to obtain the global optimal solutions of the optimization problems in (4) and (5). It is worth noting that a local optimal solution of (4) or (5) does not necessarily satisfies (2); the global optimality is crucial to ensure (2). If $C(\tau)$ is defined by (6) (i.e., Figure 1a), the optimization problems described above are formulated as *linear programming* problems. Therefore, in the previous work [27] it is straightforward to guarantee the global optimality of the proposed method. In contrast, the set in Figure 1b considered in this study is *nonconvex*. Therefore, global optimization is highly nontrivial. As a major contribution of this study, we show that the optimization problems described above can be formulated as *mixed-integer linear programming* (MILP) problems, which can be solved globally with, e.g., a branch-and-cut method.



(a)



(b)



(c)

Fig. 2: Procedure of construction of $C(\tau)$ proposed in this study. (a) To a given data set (b) we first apply the segmented least squares; (c) and next we obtain $C(\tau)$ by determining the value of τ .

In this study, we suppose that a data set such as Figure 2a is given as the result of material experiments. We first find some lines that fit this data set as shown in Figure 2b. We show that this segmented least squares can be formulated as a *mixed-integer second-order cone programming* (MISOCP) problem.¹ Next, we construct uncertainty set $C(\tau)$ shown in Figure 2c, and formulate an MILP problem to obtain a bound for the quantity of interest.

3 Segmented least squares by mixed-integer programming

This section presents segmented least squares problem that finds Figure 2b when the data set in Figure 2a is given. Section 3.1 elucidates the problem setting. Section 3.2 formulates the problem as an MISOCP problem.

3.1 Problem setting

Let $D = \{(\check{\epsilon}_1, \check{\sigma}_1), \dots, (\check{\epsilon}_r, \check{\sigma}_r)\}$ denote the data set consisting of pairs of the observed uniaxial strain and stress values. Without loss of generality, assume that the data points are numbered so that inequalities

$$\check{\epsilon}_1 < \check{\epsilon}_2 < \dots < \check{\epsilon}_r$$

are satisfied. We attempt to find at most k straight lines that best fit this data set; Figure 3 shows an example such that the data points approximately lie on either of the three straight lines. For each $i = 1, \dots, k$, define line ℓ_i by

$$\ell_i : \quad \alpha_i \epsilon + \beta_i \sigma = \gamma_i, \quad (7)$$

where $\alpha_i, \beta_i, \gamma_i \in \mathbb{R}$ are parameters that are to be determined.

This problem, the segmented least squares [30, section 6.3], can be stated formally as follows. Let $\{D_1, \dots, D_k\}$ be a partition of D , i.e., $D_1, \dots, D_k \subseteq D, D_1 \cup \dots \cup D_k = D$, and $D_i \cap D_{i'} = \emptyset$ for $i \neq i'$. Some of D_1, \dots, D_k can possibly be empty, which means that the number of straight lines used for data fitting can be less than k . The data points belonging to nonempty D_i have consecutive subscripts: In other words, with some integers l_1 and l_2 ($1 \leq l_1 \leq l_2 \leq r$), we can write

$$D_i = \{(\check{\epsilon}_{l_1}, \check{\sigma}_{l_1}), (\check{\epsilon}_{l_1+1}, \check{\sigma}_{l_1+1}), \dots, (\check{\epsilon}_{l_2-1}, \check{\sigma}_{l_2-1}), (\check{\epsilon}_{l_2}, \check{\sigma}_{l_2})\}.$$

Then we attempt fit line ℓ_i to the data points in D_i . If we adopt the least squares, then the error of the regression model for data point $(\check{\epsilon}_l, \check{\sigma}_l) \in D_i$ is given by $(\alpha_i \check{\epsilon}_l + \beta_i \check{\sigma}_l - \gamma_i)^2$. As the number of nonempty D_i 's increases (i.e., as the number of breakpoints of the regression model increases), the sum of the errors obviously decreases. Therefore, we attempt to find D_1, \dots, D_k and $\alpha_i, \beta_i, \gamma_i$ ($i = 1, \dots, k$) that minimize the sum of (i) the number of nonempty D_i 's multiplied by penalty parameter $\mu > 0$ and (ii) the sum of squared errors of ℓ_i from $(\check{\epsilon}_l, \check{\sigma}_l) \in D_i$ ($i = 1, \dots, k$). If μ is sufficiently

¹ The problem is formulated as a mixed-integer programming problem with convex quadratic constraints, which can be recast as an MISOCP problem.

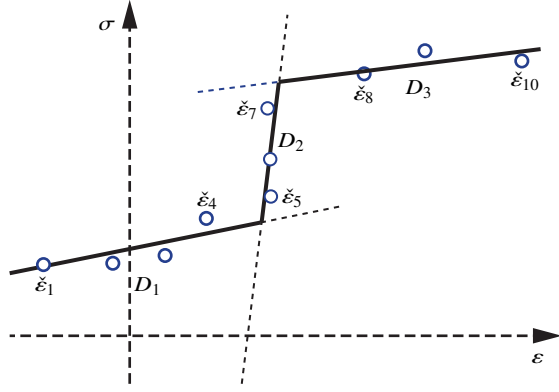


Fig. 3: Segmented least squares with three straight lines. “o” denotes the data point $(\check{\epsilon}_l, \check{\sigma}_l)$ ($l = 1, \dots, 10$) numbered as $\check{\epsilon}_1 < \check{\epsilon}_2 < \dots < \check{\epsilon}_{10}$.

large, then at the optimal solution we have $D_2 = \dots = D_k = \emptyset$ and hence our problem coincides with the conventional linear regression by the least squares. Alternatively, when $\mu > 0$ is small, the number of breakpoints of the regression model increases.

3.2 Mixed-integer programming formulation

This section presents a MIP formulation for the segmented least squares stated in section 3.1.

In the following formulation, we introduce 0-1 variables representing which one of ℓ_1, \dots, ℓ_k is fitted to each data point $(\check{\epsilon}_l, \check{\sigma}_l)$ ($l = 1, \dots, r$). Namely, for $(\check{\epsilon}_l, \check{\sigma}_l)$, we set the values of $t_{li} \in \{0, 1\}$ ($i = 1, \dots, k$) as follows:

$$(\check{\epsilon}_l, \check{\sigma}_l) \in D_i \Leftrightarrow \begin{cases} t_{l1} = \dots = t_{li} = 1, \\ t_{l,i+1} = \dots = t_{lk} = 0. \end{cases} \quad (8)$$

It is natural to fix

$$t_{1,1} = 1, \quad t_{1,2} = 0, \quad (9)$$

i.e., $(\check{\epsilon}_1, \check{\sigma}_1) \in D_1$.

Example 1 Consider the example depicted in Figure 3, where the number of data points is $r = 10$. Let $k = 5$ for example. The partition $\{D_1, \dots, D_5\}$ of D is given by

$$\begin{aligned} (\check{\epsilon}_1, \check{\sigma}_1), \dots, (\check{\epsilon}_4, \check{\sigma}_4) &\in D_1, \\ (\check{\epsilon}_5, \check{\sigma}_5), \dots, (\check{\epsilon}_7, \check{\sigma}_7) &\in D_2, \\ (\check{\epsilon}_8, \check{\sigma}_8), \dots, (\check{\epsilon}_{10}, \check{\sigma}_{10}) &\in D_3, \end{aligned}$$

and $D_4 = D_5 = \emptyset$. Correspondingly, 0-1 variables t_{li} ($l = 1, \dots, 10; i = 1, \dots, 5$) take the values

$$\begin{aligned} t_{1,1} = \dots = t_{4,1} = 1, & \quad t_{5,1} = \dots = t_{7,1} = 1, & \quad t_{8,1} = \dots = t_{10,1} = 1, \\ t_{1,2} = \dots = t_{4,2} = 0, & \quad t_{5,2} = \dots = t_{7,2} = 1, & \quad t_{8,2} = \dots = t_{10,2} = 1, \\ t_{1,3} = \dots = t_{4,3} = 0, & \quad t_{5,3} = \dots = t_{7,3} = 0, & \quad t_{8,3} = \dots = t_{10,3} = 1, \\ t_{1,4} = \dots = t_{4,4} = 0, & \quad t_{5,4} = \dots = t_{7,4} = 0, & \quad t_{8,4} = \dots = t_{10,4} = 0, \\ t_{1,5} = \dots = t_{4,5} = 0, & \quad t_{5,5} = \dots = t_{7,5} = 0, & \quad t_{8,5} = \dots = t_{10,5} = 0. \end{aligned}$$

Thus the partition of D in Figure 3 is expressed by using 0-1 variables. It is worth noting that we have to give some relations among $t_{l,1}, \dots, t_{l,10}$ to ensure that, as explained in section 3.1, the data points belonging to the same D_i should have consecutive subscripts. This motivates us to define the values of $t_{l,1}, \dots, t_{l,10}$ by (8). ■

It follows from (8) that, for each $l = 1, \dots, r$, we have

$$t_{l1} \geq t_{l2} \geq \dots \geq t_{lk}. \quad (10)$$

Since the data points in D_i should have consecutive subscripts, the constraints

$$t_{1i} \leq t_{2i} \leq \dots \leq t_{ri}$$

should be satisfied for each $i = 1, \dots, k$. Moreover, we can see that the number of nonempty ones among D_1, \dots, D_k (i.e., the number of straight lines used for data fitting) is equal to $t_{r1} + \dots + t_{rk}$.

The squared error of the regression model from data point $(\check{\varepsilon}_l, \check{\sigma}_l)$ can be expressed by using t_{il} ($i = 1, \dots, k$) as follows. For each $l = 1, \dots, r$, define $v_{l1}, \dots, v_{lk} \in \mathbb{R}$ by

$$v_{li} = \begin{cases} (\alpha_i \varepsilon_l + \beta_i \sigma_l - \gamma_i)^2 & \text{if } (t_{li}, t_{l,i+1}) = (1, 0), \\ 0 & \text{otherwise.} \end{cases} \quad (11)$$

Since (8) implies that $(t_{li}, t_{l,i+1}) = (1, 0)$ if and only if $(\check{\varepsilon}_l, \check{\sigma}_l) \in D_i$, we can write the squared error of ℓ_i from $(\check{\varepsilon}_l, \check{\sigma}_l)$ as $\sum_{i=1}^k v_{li}$. Therefore, the total error of the regression model is $\sum_{l=1}^r \sum_{i=1}^k v_{li}$. We next convert (11) into some convex constraints. Observe that constraint (10) implies that $(t_{li}, t_{l,i+1})$ takes any one of $(1, 0)$, $(0, 0)$, and $(1, 1)$. Letting M be a sufficiently large constant, we see that

$$M(1 - t_{li} + t_{l,i+1}) = \begin{cases} 0 & \text{if } (t_{li}, t_{l,i+1}) = (1, 0), \\ M & \text{if } (t_{li}, t_{l,i+1}) \in \{(0, 0), (1, 1)\}, \end{cases} \quad (12)$$

Therefore, v_{li} satisfies (11) if we minimize v_{li} under the following constraints:

$$\begin{aligned} v_{li} + M(1 - t_{li} + t_{l,i+1}) &\geq (\alpha_i \varepsilon_l + \beta_i \sigma_l - \gamma_i)^2, \\ v_{li} &\geq 0. \end{aligned}$$

It is worth noting that these two constraints are convex.

As a consequence of the discussion above, the segmented least squares in section 3.1 can be formulated as the following optimization problem:

$$\text{Minimize } \sum_{l=1}^r \sum_{i=1}^k v_{li} + \mu \sum_{i=1}^k t_{ri} \quad (13a)$$

$$\text{subject to } t_{1i} \leq \dots \leq t_{ri}, \quad i = 1, \dots, k, \quad (13b)$$

$$t_{l1} \geq \dots \geq t_{lk}, \quad l = 1, \dots, r, \quad (13c)$$

$$t_{1,1} = 1, \quad (13d)$$

$$v_{li} + M(1 - t_{li} + t_{l,i+1}) \geq (\alpha_i \varepsilon_l + \beta_i \sigma_l - \gamma_i)^2, \quad l = 1, \dots, r; i = 1, \dots, k-1, \quad (13e)$$

$$v_{lk} + M(1 - t_{lk}) \geq (\alpha_k \varepsilon_l + \beta_k \sigma_l - \gamma_k)^2, \quad l = 1, \dots, r, \quad (13f)$$

$$v_{l1}, \dots, v_{lk} \geq 0, \quad l = 1, \dots, r, \quad (13g)$$

$$t_{l1}, \dots, t_{lk} \in \{0, 1\}, \quad l = 1, \dots, r, \quad (13h)$$

$$\beta_i = 1, \quad i = 1, \dots, k. \quad (13i)$$

The optimization variables in this problem are v_{li} , t_{li} , α_i , β_i , and γ_i ($i = 1, \dots, k; l = 1, \dots, r$). Since this optimization problem is a mixed-integer programming problem with convex constraints, we can find a global optimal solution with a branch-and-cut method. Particularly, since a convex quadratic constraint can be converted to a second-order cone constraint, we can recast this problem as an MISOCP problem, for which several well-developed solvers are available. Note that constraint (13i) is a normalization of parameters α_i , β_i , and γ_i . Constraint (13d) prevents a solution with $t_{li} = 0$ and $v_{li} = 0$ ($l = 1, \dots, r; i = 1, \dots, k$) becomes optimal for problem (13).²

4 Expression and construction of uncertainty set

When we obtain the piecewise linear function in Figure 2b by using the method developed in section 3, we next construct the uncertainty set $C(\tau)$ shown in Figure 2c. This section shows that condition $(\varepsilon, \sigma) \in C(\tau)$ is equivalently rewritten as constraints that can be handled within the framework of MILP. For ease of comprehension, section 4.1 deals with the case that the result of the segmented least squares has a single breakpoint. We consider the general case in section 4.2. Section 4.3 explains the procedure for determining the value of τ .

4.1 Single breakpoint case ($k = 2$)

The lines obtained by the segmented least squares are denoted by

$$\ell_i : \alpha_i \varepsilon + \beta_i \sigma = \gamma_i, \quad i = 1, 2.$$

² We have seen that (9) ensures $(\check{\varepsilon}_1, \check{\sigma}_1) \in D_1$. However, problem (13) does not involve $t_{1,2} = 0$ as a constraint, because it is satisfied at the optimal solution by minimizing $\mu \sum_{i=1}^k t_{ri}$.

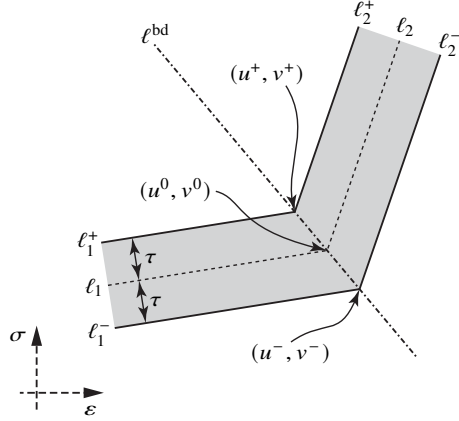


Fig. 4: Definition of set $C(\tau)$ (the gray colored part).

Here, we introduce a normalization of parameters α_i , β_i , and γ_i as follows. Let $(\alpha_i^*, \beta_i^*, \gamma_i^*)$ denote the optimal solution obtained by the method in section 3. Then we normalize it as

$$\alpha_i = \frac{\alpha_i^*}{\|(\alpha_i^*, \beta_i^*)\|}, \quad \beta_i = \frac{\beta_i^*}{\|(\alpha_i^*, \beta_i^*)\|}, \quad \gamma_i = \frac{\gamma_i^*}{\|(\alpha_i^*, \beta_i^*)\|}, \quad (14)$$

where $\|(\alpha_i^*, \beta_i^*)\|$ denotes the Euclidean norm of vector (α_i^*, β_i^*) . Moreover, without loss of generality we assume $\alpha_i < 0$.

Define $C(\tau) \subset \mathbb{R}^2$ as depicted in Figure 4, where the border lines are obtained by shifting ℓ_1 and ℓ_2 by distance τ ; the precise definition of $C(\tau)$ will be given by (18). We use ℓ_i^- and ℓ_i^+ to denote the lines consisting of the border of $C(\tau)$, where

$$\ell_i^- : \alpha_i \varepsilon + \beta_i \sigma = \gamma_i - \tau, \quad i = 1, 2, \quad (15)$$

$$\ell_i^+ : \alpha_i \varepsilon + \beta_i \sigma = \gamma_i + \tau, \quad i = 1, 2. \quad (16)$$

Let (u^-, v^-) denote the intersection point of ℓ_1^- and ℓ_2^- , and (u^+, v^+) denote the intersection point of ℓ_1^+ and ℓ_2^+ ; see Figure 4. We use $(u^0, v^0) \in \mathbb{R}^2$ to denote the intersection point of ℓ_1 and ℓ_2 . Let ℓ^{bd} denote the line passing through (u^-, v^-) , (u^0, v^0) , and (u^+, v^+) , and write it as

$$\ell^{\text{bd}} : p\varepsilon + q\sigma = r. \quad (17)$$

In the expression above, $p, q, r \in \mathbb{R}$ are constants that will be computed concretely in the following. We see that $C(\tau)$ is a set of points $(\varepsilon, \sigma) \in \mathbb{R}^2$ satisfying³

$$\begin{cases} |\alpha_1 \varepsilon + \beta_1 \sigma - \gamma_1| \leq \tau & \text{if } p\varepsilon + q\sigma \leq r, \\ |\alpha_2 \varepsilon + \beta_2 \sigma - \gamma_2| \leq \tau & \text{if } p\varepsilon + q\sigma \geq r; \end{cases} \quad (18)$$

see Figure 4 and Figure 5.

³ Inclusion of condition $p\varepsilon + q\sigma = r$ in the both two cases of (18) does not matter.

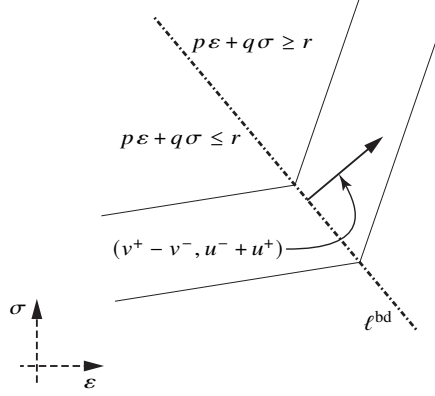


Fig. 5: Case division in (18).

We are now in position to compute the values of p , q , and r for ℓ^{bd} in (17); see Figure 5. Observe that ℓ^{bd} is in parallel with vector $(u^+ - u^-, v^+ - v^-)$ (namely, is orthogonal to vector $(v^+ - v^-, -u^+ + u^-)$), and passes through point (u^0, v^0) . Hence, it is written as

$$(v^+ - v^-)(\varepsilon - u^0) - (u^+ - u^-)(\sigma - v^0) = 0. \quad (19)$$

An elementary calculation shows that u^0 , v^0 , $u^+ - u^-$, and $v^+ - v^-$ are given by

$$u^0 = \frac{\beta_2 \gamma_1 - \beta_1 \gamma_2}{\alpha_1 \beta_2 - \alpha_2 \beta_1}, \quad (20)$$

$$v^0 = \frac{\alpha_1 \gamma_2 - \alpha_2 \gamma_1}{\alpha_1 \beta_2 - \alpha_2 \beta_1}, \quad (21)$$

$$u^+ - u^- = \frac{2(\beta_2 - \beta_1)\tau}{\alpha_1 \beta_2 - \alpha_2 \beta_1}, \quad (22)$$

$$v^+ - v^- = \frac{2(\alpha_1 - \alpha_2)\tau}{\alpha_1 \beta_2 - \alpha_2 \beta_1}. \quad (23)$$

Substitute (20), (21), (22), and (23) into (19) to see that p , q , and r in (17) are obtained as

$$p = \alpha_1 - \alpha_2, \quad (24)$$

$$q = \beta_1 - \beta_2, \quad (25)$$

$$r = pu^0 + qv^0. \quad (26)$$

We next introduce a 0-1 variable s , and make it correspond to the case division in (18) as⁴

$$s = 0 \quad \leftrightarrow \quad p\varepsilon + q\sigma \leq r, \quad (27)$$

$$s = 1 \quad \leftrightarrow \quad p\varepsilon + q\sigma \geq r. \quad (28)$$

⁴ In a manner similar to (18), in (28) condition $p\varepsilon + q\sigma = r$ corresponds to both $s = 0$ and $s = 1$, which is of no matter for the following formulations.

Accordingly, the inequalities on the left side of (18) correspond to s as

$$s = 0 \quad \leftrightarrow \quad |\alpha_1 \varepsilon + \beta_1 \sigma - \gamma_1| \leq \tau, \quad (29)$$

$$s = 1 \quad \leftrightarrow \quad |\alpha_2 \varepsilon + \beta_2 \sigma - \gamma_2| \leq \tau. \quad (30)$$

Thus, (18) is equivalently restated as (27), (28), (29), and (30). The remaining concern is to reduce these four conditions to some linear inequalities. To this end, we use a sufficiently large constant M . Then conditions (27) and (28) are equivalently rewritten as

$$p\varepsilon + q\sigma \leq r + Ms, \quad (31)$$

$$p\varepsilon + q\sigma \geq r - M(1 - s). \quad (32)$$

We also see that conditions (29) and (30) are equivalently rewritten as

$$|\alpha_1 \varepsilon + \beta_1 \sigma - \gamma_1| \leq \tau + Ms, \quad (33)$$

$$|\alpha_2 \varepsilon + \beta_2 \sigma - \gamma_2| \leq \tau + M(1 - s). \quad (34)$$

As a consequence of this section, we obtain

$$(\varepsilon, \sigma) \in C(\tau) \quad \Leftrightarrow \quad \exists s \in \{0, 1\} : (31), (32), (33), (34).$$

It is worth noting that the constraints on the right side of this expression can be treated within the framework of MILP.

4.2 General case ($k \geq 3$)

This section generalizes the analysis in section 4.1 to the case in which the result of the segmented least squares has k lines with $k - 1$ breakpoints.

As the output of the segmented least squares, we obtain lines ℓ_1, \dots, ℓ_k . We use the normalization of $\alpha_i, \beta_i, \gamma_i$ ($i = 1, \dots, k$) in (14), and assume $\alpha_i < 0$ without loss of generality. Let (u_i^0, v_i^0) denote the intersection point of ℓ_i and ℓ_{i+1} ($i = 1, \dots, k - 1$). A simple calculation shows

$$(u_i^0, v_i^0) = \left(\frac{\beta_{i+1}\gamma_i - \beta_i\gamma_{i+1}}{\alpha_i\beta_{i+1} - \alpha_{i+1}\beta_i}, \frac{\gamma_{i+1}\alpha_i - \gamma_i\alpha_{i+1}}{\alpha_i\beta_{i+1} - \alpha_{i+1}\beta_i} \right). \quad (35)$$

The lines consisting of the border of $C(\tau)$, denoted by ℓ_i^- and ℓ_i^+ ($i = 1, \dots, k$), are defined in the same manner as (15) and (16). Define $p_i, q_i, r_i \in \mathbb{R}$ ($i = 1, \dots, k - 1$) by

$$p_i = \alpha_i - \alpha_{i+1}, \quad (36)$$

$$q_i = \beta_i - \beta_{i+1}, \quad (37)$$

$$r_i = p_i u_i^0 + q_i v_i^0. \quad (38)$$

Lines defined by $p_i\varepsilon + q_i\sigma = r_i$ ($i = 1, \dots, k-1$) play a role similar to ℓ^{bd} in section 4.1; see Figure 4 and Figure 5. For simplicity of notation, let

$$p_0 = 0, \quad q_0 = 0, \quad r_0 = 0, \quad (39)$$

$$p_k = 0, \quad q_k = 0, \quad r_k = 0. \quad (40)$$

We see that $C(\tau)$ is the set of points satisfying

$$|\alpha_i\varepsilon + \beta_i\sigma - \gamma_i| \leq \tau \iff p_{i-1}\varepsilon + q_{i-1}\sigma \geq r_{i-1}, \quad p_i\varepsilon + q_i\sigma \leq r_i, \\ i = 1, \dots, k. \quad (41)$$

We next introduce 0-1 variables $s_1, \dots, s_{k-1} \in \{0, 1\}$ to express the case divisions in (41) as

$$s_1 = \dots = s_{i-1} = 1, \quad s_i = \dots = s_{k-1} = 0 \\ \iff p_{i-1}\varepsilon + q_{i-1}\sigma \geq r_{i-1}, \quad p_i\varepsilon + q_i\sigma \leq r_i \quad (42)$$

for each $i = 1, \dots, k-1$. In this expression, we see that the 0-1 variables satisfy

$$s_1 \geq s_2 \geq \dots \geq s_{k-1}. \quad (43)$$

The inequality on the left side of (41) is linked to the 0-1 variables as

$$s_1 = \dots = s_{i-1} = 1, \quad s_i = \dots = s_{k-1} = 0 \\ \iff |\alpha_i\varepsilon + \beta_i\sigma - \gamma_i| \leq \tau \quad (44)$$

for each $i = 1, \dots, k$. Thus, $C(\tau)$ in (41) is equivalently expressed as (42) and (44). Observe that the relation in (42) can be rewritten as the linear inequalities

$$p_{i-1}\varepsilon + q_{i-1}\sigma \geq r_{i-1} - M(i-1 - s_1 - \dots - s_{i-1} + s_i + \dots + s_{k-1}), \\ i = 1, \dots, k, \quad (45)$$

$$p_i\varepsilon + q_i\sigma \leq r_i + M(i-1 - s_1 - \dots - s_{i-1} + s_i + \dots + s_{k-1}), \\ i = 1, \dots, k. \quad (46)$$

Similarly, the relation in (44) can be rewritten as the following linear inequalities:

$$|\alpha_i\varepsilon + \beta_i\sigma - \gamma_i| \leq \tau + M(i-1 - s_1 - \dots - s_{i-1} + s_i + \dots + s_{k-1}), \\ i = 1, \dots, k. \quad (47)$$

As a consequence, point $(\varepsilon, \sigma) \in \mathbb{R}^2$ satisfies (41) (i.e., $(\varepsilon, \sigma) \in C(\tau)$) if and only if there exist $(s_1, \dots, s_{k-1}) \in \{0, 1\}^k$ satisfying (43), (45), (46), and (47).

4.3 Determination of τ

This section describes the procedure for determining the value of τ for $C(\tau)$. Recall that the data set D consists of r data points. When we choose the values of ϵ and δ in (2), \bar{p} is determined as the smallest integer satisfying (3). Then τ is to be determined so that the number of data points that are included in $C(\tau)$ is equal to \bar{p} . We can use a bisection method for finding this value of τ .

The bisection method demands the following preparation. We have the output, $(\alpha_i, \beta_i, \gamma_i)$ ($i = 1, \dots, k$), of the segmented least squares. Compute u_i^0, v_i^0 ($i = 1, \dots, k-1$) by (35). Moreover, compute p_i, q_i, r_i ($i = 0, 1, 2, \dots, k$) by (36), (37), (38), (39), and (40). Define $D_i \subset \mathbb{R}^2$ ($i = 1, \dots, k$) by

$$D_i = \{(\epsilon, \sigma) \in \mathbb{R}^2 \mid p_{i-1}\epsilon + q_{i-1}\sigma \geq r_{i-1}, p_i\epsilon + q_i\sigma \leq r_i\}.$$

Then, for each $l = 1, \dots, k$, find $i_l \in \{1, \dots, k\}$ such that $(\check{\epsilon}_l, \check{\sigma}_l) \in D_{i_l}$ holds.

Algorithm 1 describes the bisection method for computing τ .

Algorithm 1 Bisection method for computing τ .

Require: i_l ($l = 1, \dots, r$), \bar{p} , $\tau_{\max} > 0$, $\epsilon_{\text{bi}} > 0$.

```

1:  $\tau \leftarrow \tau_{\max}$ ,  $\tau_{\min} \leftarrow 0$ .
2: while  $\tau_{\max} - \tau_{\min} \geq \epsilon_{\text{bi}}$  do
3:    $\tau \leftarrow (\tau_{\max} + \tau_{\min})/2$ ,  $p \leftarrow 0$ .
4:   for  $l = 1, \dots, r$  do
5:     if  $|\alpha_{i_l} \check{\epsilon}_l + \beta_{i_l} \check{\sigma}_l - \gamma_{i_l}| \leq \tau$  then
6:        $p \leftarrow p + 1$ .
7:     end if
8:   end for
9:   if  $p \geq \bar{p}$  then
10:     $\tau_{\max} \leftarrow \tau$ .
11:   else
12:     $\tau_{\min} \leftarrow \tau$ .
13:   end if
14: end while

```

5 Formulation for trusses

By adopting $C(\tau)$ formulated in section 4, we can compute lower and upper bounds for the structural response that satisfy (2). In this section, taking trusses for example, we show that the optimization problems for computing these lower and upper bounds can be recast as MILP problems. It is worth noting that we can solve an MILP problem globally with, e.g., a branch-and-cut method. Guaranteeing the global optimality is crucial to finding a bound for the structural response, because a local optimal solution in general underestimates the structural response; the global optimality ensures (2).

Consider a truss that undergoes small deformation. The constitutive law relates the uniaxial strain $\epsilon \in \mathbb{R}$ to the uniaxial stress $\sigma \in \mathbb{R}$. Let d denote the number of degrees of freedom of the nodal displacements of the truss. We use $\mathbf{u} \in \mathbb{R}^d$ and $\mathbf{f} \in \mathbb{R}^d$ to denote

the vectors of the nodal displacements and the nodal external forces, respectively. Let m denote the number of truss members. For member e ($e = 1, \dots, m$), we use $\sigma_e \in \mathbb{R}$ and $\varepsilon_e \in \mathbb{R}$ to denote its stress and strain, respectively, and write $\boldsymbol{\varepsilon} = (\varepsilon_e) \in \mathbb{R}^m$ and $\boldsymbol{\sigma} = (\sigma_e) \in \mathbb{R}^m$. The compatibility relations and the force-balance equations can be written in the forms

$$\begin{aligned}\boldsymbol{\varepsilon} &= L\mathbf{u}, \\ N\boldsymbol{\sigma} &= \mathbf{f},\end{aligned}$$

where $L \in \mathbb{R}^{m \times d}$ and $N \in \mathbb{R}^{d \times m}$ are constant matrices.

We obtain the uncertainty set, $C(\tau)$, by using the method presented in section 4. Then we can see from the fact reviewed in section 2.1 that $C(\tau)$ satisfies

$$\mathbb{P}_F\{\mathbb{P}\{(\boldsymbol{\varepsilon}, \boldsymbol{\sigma}) \in C(\tau)\} \geq 1 - \epsilon\} \geq 1 - \delta.$$

Let $q(\mathbf{u}, \boldsymbol{\sigma})$ denote the quantity of interest. Then a lower bound for the quantity of interest, \underline{q} , can be obtained as the optimal value of the following optimization problem:

$$\text{Minimize } q(\mathbf{u}, \boldsymbol{\sigma}) \quad (48a)$$

$$\text{subject to } \boldsymbol{\varepsilon} = L\mathbf{u}, \quad (48b)$$

$$N\boldsymbol{\sigma} = \mathbf{p}, \quad (48c)$$

$$(\varepsilon_e, \sigma_e) \in C(\tau), \quad e = 1, \dots, m. \quad (48d)$$

It is crucial in the formulation above that constraint

$$(\varepsilon_e, \sigma_e) \in C(\tau) \quad (49)$$

for each $e = 1, \dots, m$ can be equivalently rewritten into some linear inequalities by introducing some 0-1 variables.

We next present the concrete reformulation of constraint (49). As an example, suppose that the number of straight lines of the output of the segmented least squares is $k = 3$ (i.e., the number of breakpoints is two). We use the result established in section 4.2. For each member e ($e = 1, \dots, m$), we introduce two 0-1 variables, s_{e1} and s_{e2} . Then we can reformulate (49) equivalently as follows:

$$s_{e1} \geq s_{e2}, \quad (50)$$

$$p_1\varepsilon_e + q_1\sigma_e \leq r_1 + M(s_{e1} + s_{e2}), \quad (51)$$

$$p_1\varepsilon_e + q_1\sigma_e \geq r_1 - M(1 - s_{e1} + s_{e2}), \quad (52)$$

$$p_2\varepsilon_e + q_2\sigma_e \leq r_2 + M(1 - s_{e1} + s_{e2}), \quad (53)$$

$$p_2\varepsilon_e + q_2\sigma_e \geq r_2 - M(2 - s_{e1} - s_{e2}), \quad (54)$$

$$|\alpha_1\varepsilon_e + \beta_1\sigma_e - \gamma_1| \leq d + M(s_{e1} + s_{e2}), \quad (55)$$

$$|\alpha_2\varepsilon_e + \beta_2\sigma_e - \gamma_2| \leq d + M(1 - s_{e1} + s_{e2}), \quad (56)$$

$$|\alpha_3\varepsilon_e + \beta_3\sigma_e - \gamma_3| \leq d + M(2 - s_{e1} - s_{e2}), \quad (57)$$

$$s_{e1}, s_{e2} \in \{0, 1\}. \quad (58)$$

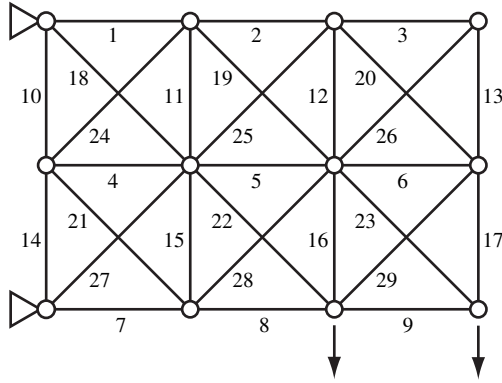


Fig. 6: Problem setting of the truss example.

Thus, we can replace constraint (48d) of problem (48) with (50), (51), (52), (53), (54), (55), (56), (57), and (58) for each $e = 1, \dots, m$. The optimization problem is thence an MILP problem when the objective function q is a linear function (that is often the case as seen in section 6). Accordingly, we can find the global optimal solution of problem (48), which corresponds to a conservative prediction \underline{q} satisfying (2).

An upper bound for the quantity of interest, \bar{q} , can be found by maximizing q under the same constraints.

6 Numerical examples

This section demonstrates three numerical examples.⁵ The proposed method was implemented on MATLAB ver. 23.2. We used CPLEX ver. 12.9 [16] to solve MILP and MISOCP problems. For MISOCP problems, we set the MIQCPstrategy parameter of CPLEX so that linear programming relaxations are adopted, rather than relaxations with convex quadratic constraints. The numerical experiments were conducted on a 2.6 GHz Intel Core i7 processor with 32 GB RAM.

6.1 Truss example

Consider a planar truss shown in Figure 6. This truss consists of $m = 29$ members and has $d = 20$ degrees of freedom of the nodal displacements. The lengths of horizontal and vertical members are 1 m. The cross-sectional area of each member is 1000 mm^2 . We apply the external vertical downward forces of $2.1\lambda \text{ kN}$ at the bottom two nodes as shown in Figure 6, where $\lambda \in \mathbb{R}$ is the load factor.

Suppose that we are given the material data set shown in Figure 7, which consists of $r = 200$ data points. Figure 8 shows the optimal solution of the segmented least

⁵ The main MATLAB codes and the data sets used in the analysis of this section are available at https://github.com/ykanno22/re1_comp_segmented/.

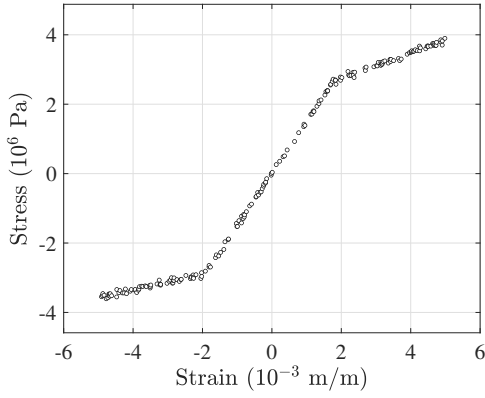


Fig. 7: Data set for the truss example.

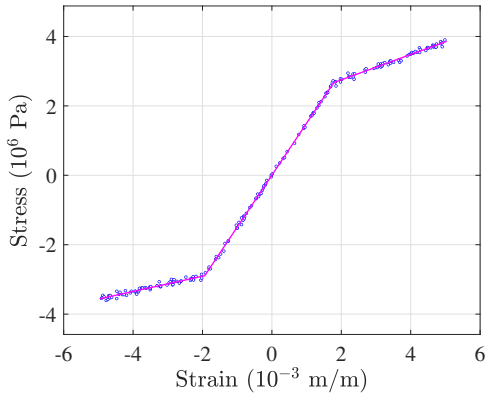


Fig. 8: Result of the segmented least squares for the data set in Figure 7.

squares with $k = 5$, $\mu = 2.0$, and $M = 1.0 \times 10^3$. We can observe that the penalty for the number of lines works substantially: Although five straight lines can be used for fitting the data, the optimal solution uses only three lines and fits the data very well.

In accordance with the result of the segmented least squares in Figure 8, we put $k = 3$ in the following. We specify the target reliability and confidence level as $1 - \epsilon = 0.9$ and $1 - \delta = 0.9$, respectively. The uncertainty set, $C(\tau)$, is then determined by Algorithm 1 with $\epsilon_{bi} = 10^{-7}$. To find a bound for the structural response, we employ the MILP formulation in section 5 with $M = 1.0 \times 10^2$. As for the quantity of interest, we first adopt the vertical displacement of the rightmost bottom node of the truss. Figure 9 reports the solutions obtained by the proposed method, where the obtained bounds are shown for several different values of the load factor, λ . As for a reference solution, we use the result of the segmented least squares in Figure 8 as the constitutive law, and perform the conventional equilibrium analysis.⁶ These reference solutions are also shown in Figure 9 as “□”. For each value of λ , we can observe that the

⁶ We adopt MATLAB built-in function `fsolve` as a solver for a system of nonlinear equations.

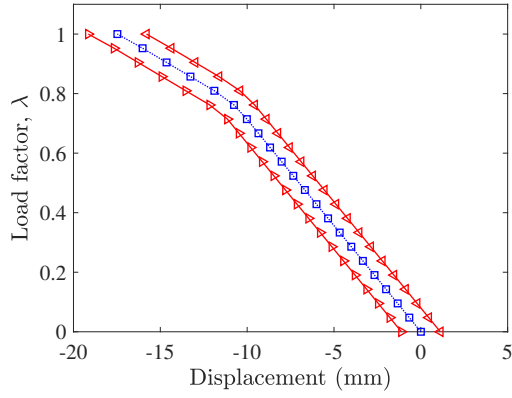


Fig. 9: Bounds for the nodal displacement of the truss. “◄” and “►” denote the upper and lower bounds obtained by the proposed method, respectively; “□” denotes the reference solution.

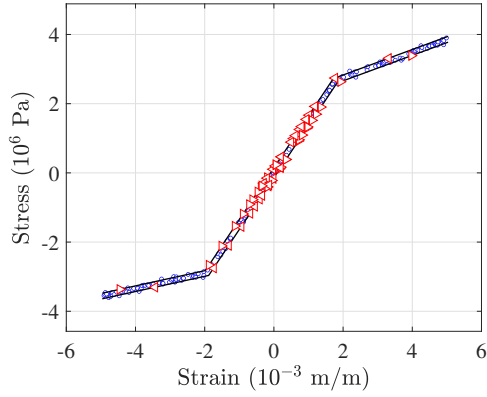


Fig. 10: Member stresses–strains corresponding to the obtained solutions at $\lambda = 1$ in Figure 9. Boundary of the uncertainty set $C(\tau)$ is also depicted. “◄” and “►” denote the member stresses corresponding to the upper and lower bound solutions, respectively.

reference solution belongs to the obtained interval, which supports the rationality of the proposed method. Figure 10 shows the boundary of $C(\tau)$, and plots $(\varepsilon_e, \sigma_e)$ ($e = 1, \dots, m$) corresponding to the obtained upper and lower bounds for $\lambda = 1$. We can confirm $(\varepsilon_e, \sigma_e) \in C(\tau)$ for all the members.

We next focus attention to the member stresses at $\lambda = 1$. Figure 11 shows the upper and lower bounds obtained by the proposed method as well as the reference solutions, where the member indices are defined in Figure 6.

Figure 12a reports the variation of the interval bound for the stress of member 1 with respect to the confidence level $1 - \delta$, with $\epsilon = 0.1$ being fixed. As the required confidence level becomes higher, the interval guaranteeing the reliability $1 - \epsilon$ becomes wider. Similarly, Figure 12b reports the variation of the interval bound with respect to

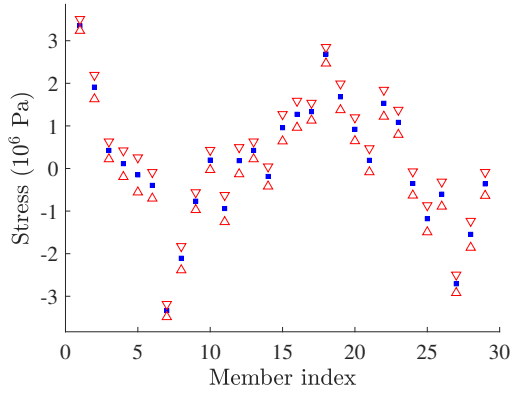


Fig. 11: Bounds for the member stresses of the truss example. “ ∇ ” and “ Δ ” denote the upper and lower bounds obtained by the proposed method, respectively. “ \blacksquare ” denotes the reference solution.

the target reliability $1 - \epsilon$, with δ being fixed. As the target reliability becomes higher, the interval with the required confidence level becomes wider.

6.2 Frame example

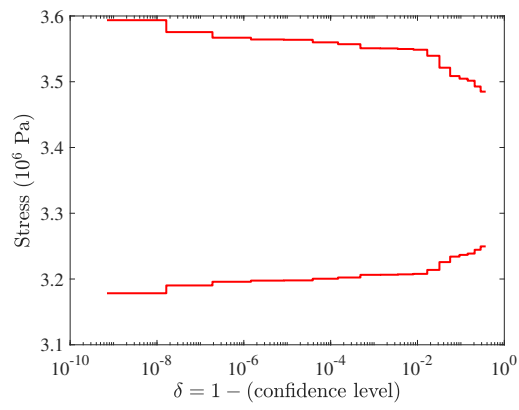
Consider the planar frame structure illustrated in Figure 13. The equilibrium analysis of the frame structure is based on the formulation in [20]. The top two nodes are fixed, and the frame has $m = 12$ members and $d = 18$ degrees of freedom of the nodal displacements. As for the external load, we apply a vertical downward force of 2.4λ kN at the rightmost node, where $\lambda \in [0, 1]$ is the load factor. Each member has a hollow circular cross-section, and the cross-sectional area of each member is 1000 mm^2 . The moment of inertia is computed by supposing that the ratio of the inertial radius to the external radius is 0.9.

Figure 14 shows the material data set consisting of $r = 80$ data points. Figure 15 reports the result of the segmented least squares with $k = 5$, $\mu = 2.0$, and $M = 1.0 \times 10^3$. We see that the optimal solution uses three straight lines to fit the data.

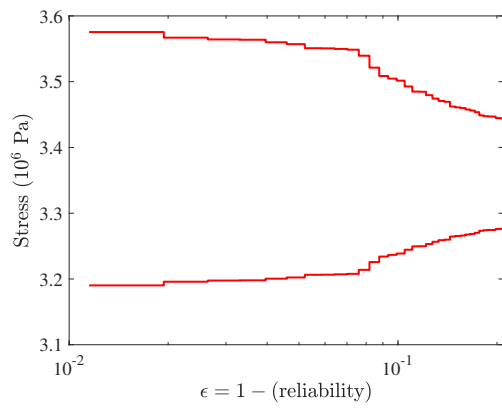
We set the target reliability and confidence level to $1 - \epsilon = 0.9$ and $1 - \delta = 0.9$, respectively. We adopt the vertical displacement of the rightmost node as the quantity of interest. Figure 16 reports the interval bounds obtained by the proposed method, as well as the reference solutions, for different values of the load factor λ . Figure 17 plots $(\varepsilon_e, \sigma_e)$ ($e = 1, \dots, m$) corresponding to the upper and lower bound solutions at $\lambda = 1$, as well as the boundary of $C(\tau)$.

6.3 Cable–strut structure example

Consider the three-dimensional pin-jointed structure shown in Figure 18. This structure consists of 12 cables (depicted as the thin lines) and 3 struts (depicted as the



(a)



(b)

Fig. 12: Variations of the upper and lower bounds for the stress of member 1 in the truss example. (a) $\epsilon = 0.1$; and (b) $\delta = 0.1$.

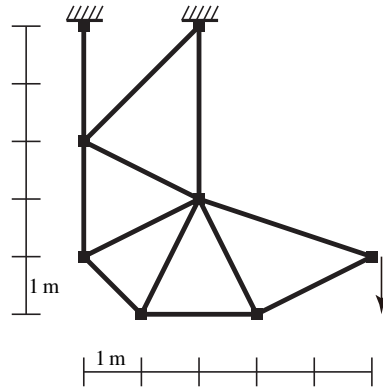


Fig. 13: Problem setting of the frame example.

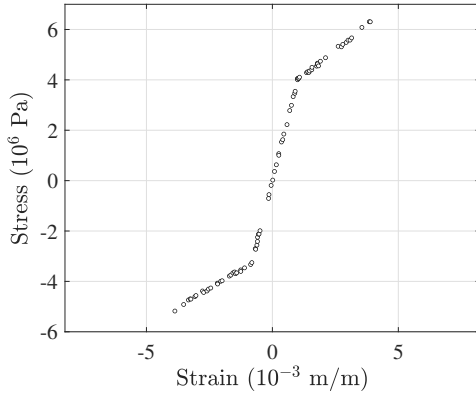


Fig. 14: Data set for the frame example.

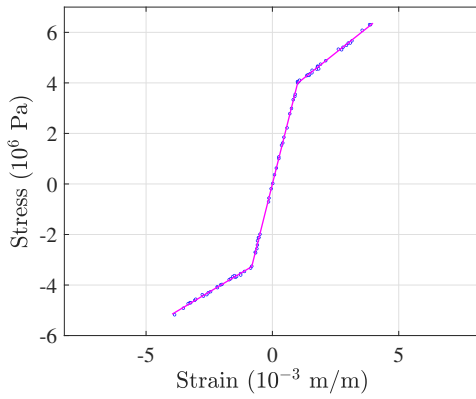


Fig. 15: Result of the segmented least squares for the data set in Figure 14.

thick lines). The bottom and top layers are equilateral triangles consisting of three cables, where the length of each cable is $\sqrt{3}$ m. The bottom layer is in parallel with the top layer with $\pi/4$ rad rotated position. The distance between these two layers is 1.5 m. The length of each strut is 2.4863 m. The cross-sectional areas of the cables and struts are 500 mm^2 and 1000 mm^2 , respectively. To prevent the rigid-body motion, we fix 6 degrees of freedom of the displacements of the bottom nodes. Accordingly, the number of degrees of freedom of the nodal displacements is $d = 12$. As for the external load, we apply the vertical downward forces of $1.1\lambda \text{ kN}$ at the three top nodes, where $\lambda \in \mathbb{R}$ is the load factor. As the initial strains, at the nodal location above each cable and each strut have strains of 2×10^{-3} and -0.4×10^{-3} , respectively. It is worth noting that the nodal location above is not the self-equilibrium shape.

Figure 19 collects the material data sets. For cables we use the one in Figure 19a, which consists of 150 data points. Moreover, for struts we use the one in Figure 19b, which consists of 80 data points. To each data set we apply the segmented least squares with $k = 5$, $\mu = 2.0$, and $M = 1.0 \times 10^3$. In both cases, the optimal solution uses

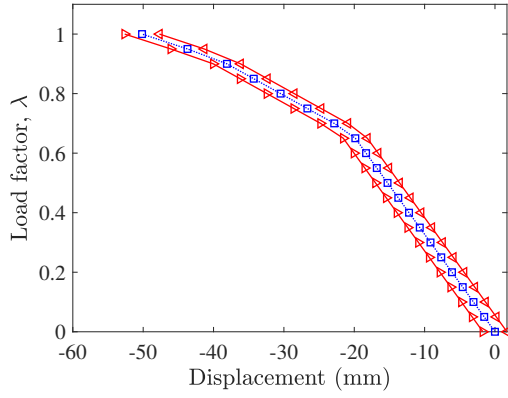


Fig. 16: Bounds for the nodal displacement of the frame. “◁” and “▷” denote the upper and lower bounds obtained by the proposed method, respectively; “◻” denotes the reference solution.

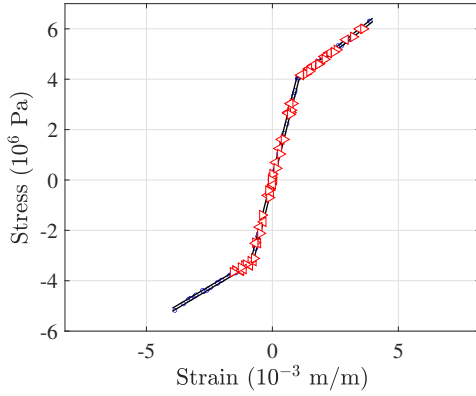


Fig. 17: Member stresses–strains corresponding to the obtained solutions at $\lambda = 1$ in Figure 16. Boundary of the uncertainty set $C(\tau)$ is also depicted. “◁” and “▷” denote the member stresses corresponding to the upper and lower bound solutions, respectively.

three straight lines (i.e., it has two breakpoints). By using these results, we compute the reference solutions of the equilibrium analysis.

We set $\epsilon = 0.1$ and $\delta = 0.1$. The quantity of interest is the vertical displacement of a top node. Figure 20 reports the interval bounds obtained by the proposed method, as well as the reference solutions. As the load factor λ increases, the stiffnesses of some cable members can be very close to 0, and hence the interval becomes wider. It is confirmed that the reference solution always belongs to the obtained interval. Figure 21 plots (ϵ_e, σ_e) ($e = 1, \dots, m$) corresponding to the upper and lower bound solutions at $\lambda = 1$, as well as the boundary of $C(\tau)$. Particularly, we can observe in

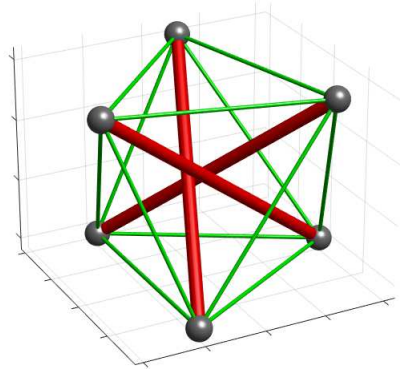


Fig. 18: Problem setting of the cable–strut structure example.

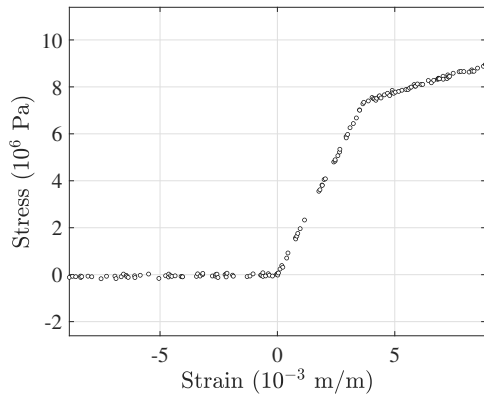
Figure 21a that some cables undergo large compression deformations at the lower bound solution.

Figure 22 reports the computation costs of solving the MILP problems for obtaining the solutions shown in Figure 20. Figure 22a and 22b shows the computation time and the number of enumeration nodes of CPLEX, respectively. We can observe that the computation cost is irrelevant to the stiffnesses of the cable members.

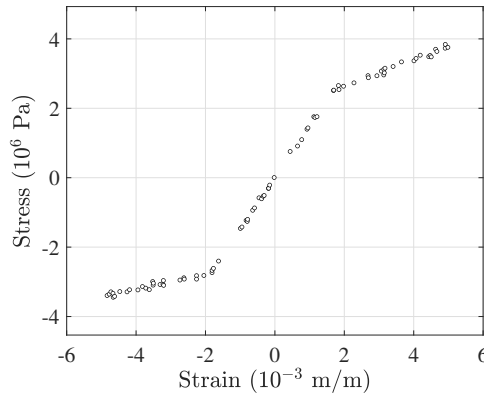
7 Conclusions

This paper has presented an optimization-based method, within the framework of data-driven computational elasticity, for computing a bound of the structural response considering the uncertainty in the material data set. The method ensures that, at least the specified confidence level, the probability that the structural response is within the obtained bound is no smaller than the target reliability. This guarantee is provided by a fundamental property of the order statistics. This means that the proposed method is free from modeling of the probabilistic distribution of the constitutive law, and hence this method can be viewed as a purely data-driven approach.

The method developed in this paper is a natural extension of the previous work [27], which has a drawback that its solution overestimates the structural response drastically when the stress–strain relation in the given material data set is not approximately linear. To deal with such a data, this paper has presented a method consisting of two steps: We first apply the segmented least squares to the data set; then with constructing the uncertainty set based on the order statistics we solve optimization problems to find the structural bound. In this paper we have shown that the optimization problems in both steps can be formulated as mixed-integer convex optimization problems, which can be solved globally. The guarantee of the global optimality in the latter step is particularly



(a)



(b)

Fig. 19: Data sets for the cable–strut structure example. (a) Data set for cables; and (b) data set for struts.

crucial, because a bound corresponding to a local optimal solution underestimates the structural response in general. Besides this method, the global optimality is guaranteed in the approaches in [27] and [8], which aim at handling a almost linear stress–strain relation. In contrast, the method in [13] proposed for dealing with nonlinearity lacks guarantee of the global optimality.

Numerical examples have been demonstrated for three skeletal structures: A truss, frame, and cable–strut structure. We have compared the interval bounds obtained by the proposed method with the reference solutions to confirm validity of the method. Since the optimization problems in these examples were solved within a few minutes by a standard solver, the computation cost required by the proposed method is practically acceptable. In contrast, if the given data set fits well a nonlinear smooth curve, rather than a piecewise-affine function, then the number of 0-1 variables in the proposed formulations increases, which can possibly yield drastic increase of computation cost. It is worth noting that, besides the structural types in the numerical examples presented

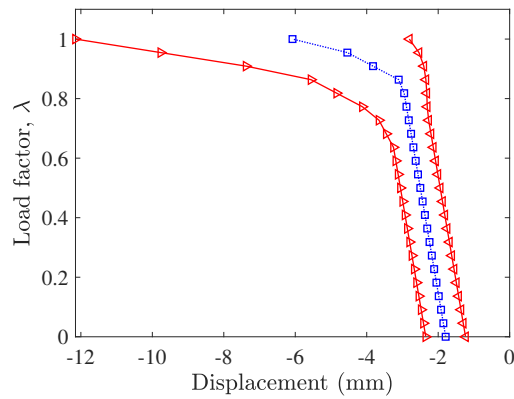


Fig. 20: Bounds for the nodal displacement of the cable–strut structure. “ \triangleleft ” and “ \triangleright ” denote the upper and lower bounds obtained by the proposed method, respectively. “ \square ” denote the reference solution.

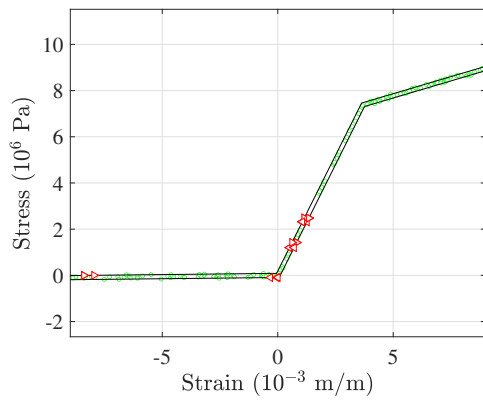
in this paper, we can apply the proposed method to space frames, provided that a data set of pairs of shear stresses and shear strains is also given. An extension to general continua remains as future work.

Acknowledgments This work is partially supported by JST CREST Grant Number JPMJCR1911, Japan, and JSPS KAKENHI JP21K04351 and 24K07747.

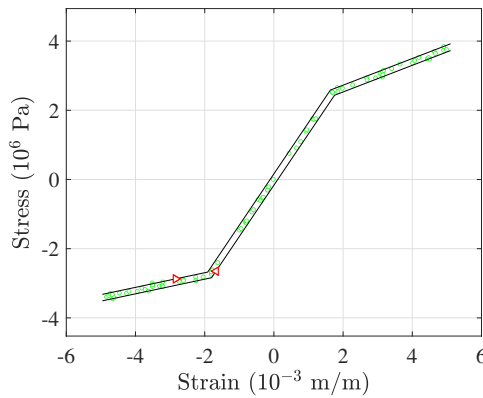
Conflict of interest The author declares that there is no conflict of interest.

References

1. P. Carrara, L. De Lorenzis, L. Stainier, M. Ortiz: Data-driven fracture mechanics. *Computer Methods in Applied Mechanics and Engineering*, **372**, 113390 (2020).
2. K. Ciftci, K. Hackl: Model-free data-driven simulation of inelastic materials using structured data sets, tangent space information and transition rules. *Computational Mechanics*, **70**, 425–435 (2022).
3. A. Clément, C. Soize, J. Yvonnet: Computational nonlinear stochastic homogenization using a non-concurrent multiscale approach for hyperelastic heterogeneous microstructures analysis. *International Journal for Numerical Methods in Engineering*, **91**, 799–824 (2012).
4. M. Dalémat, M. Coret, A. Leygue, E. Verron: Measuring stress field without constitutive equation. *Mechanics of Materials*, **136**, 103087 (2019).
5. H. Dandin, A. Leygue, L. Stainier: Graph-based representation of history-dependent material response in the data-driven computational mechanics framework. *Computer Methods in Applied Mechanics and Engineering*, **419**, 116694 (2024).
6. R. Eggersmann, T. Kirchdoerfer, S. Reese, L. Stainier, M. Ortiz: Model-free data-driven inelasticity. *Computer Methods in Applied Mechanics and Engineering*, **350**, 81–99 (2019).
7. R. Ghanem, D. Higdon, H. Owhadi (eds.): *Handbook of Uncertainty Quantification*. Springer International Publishing, Cham (2017).
8. X. Guo, Z. Du, C. Liu, S. Tang: A new uncertainty analysis-based framework for data-driven computational mechanics. *Journal of Applied Mechanics*, **88**, 111003 (2021).
9. Y. Guo, Z. Du, L. Wang, W. Meng, T. Zhang, R. Su, D. Yang, S. Tang, X. Guo: Data-driven topology optimization (DDTO) for three-dimensional continuum structures. *Structural and Multidisciplinary Optimization*, **66**, 104 (2023).



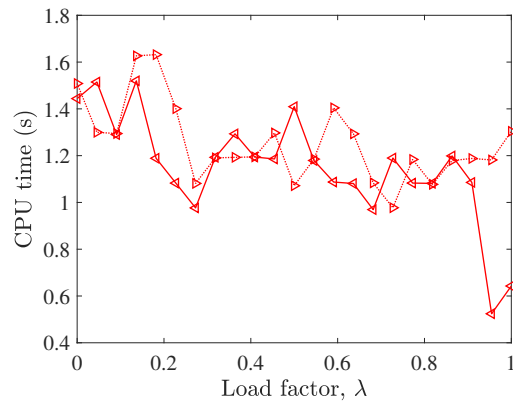
(a)



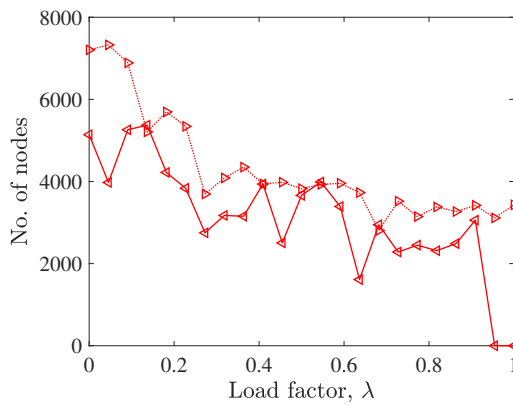
(b)

Fig. 21: Member stresses–strains corresponding to the obtained solutions at $\lambda = 1$ in Figure 20. Boundary of the uncertainty set $C(\tau)$ is also depicted. “ \triangleleft ” and “ $\triangle>$ ” denote the member stresses corresponding to the upper and lower bound solutions, respectively. (a) Cables; and (b) struts.

10. P. Hao, H. Yang, H. Yang, Y. Zhang, Y. Wang, B. Wang: A sequential single-loop reliability optimization and confidence analysis method. *Computer Methods in Applied Mechanics and Engineering*, **399**, 115400 (2022).
11. Q. He, J.-S. Chen: A physics-constrained data-driven approach based on locally convex reconstruction for noisy database. *Computer Methods in Applied Mechanics and Engineering*, **363**, 112791 (2020).
12. Q. He, D. W. Laurence, C.-H. Lee, J.-S. Chen: Manifold learning based data-driven modeling for soft biological tissues. *Journal of Biomechanics*, **117**, 110124 (2021).
13. M. Huang, C. Liu, Z. Du, S. Tang, X. Guo: A sequential linear programming (SLP) approach for uncertainty analysis-based data-driven computational mechanics. *Computational Mechanics*, to appear. DOI: [10.1007/s00466-023-02395-8](https://doi.org/10.1007/s00466-023-02395-8).
14. R. Ibañez, E. Abisset-Chavanne, J. V. Aguado, D. Gonzalez, E. Cueto, F. Chinesta: A manifold learning approach to data-driven computational elasticity and inelasticity. *Archives of Computational Methods in Engineering*, **25**, 47–57 (2018).
15. R. Ibañez, D. Borzacchiello, J. V. Aguado, E. Abisset-Chavanne, E. Cueto, P. Ladeveze, F. Chinesta: Data-driven non-linear elasticity: constitutive manifold construction and problem discretization. *Com-*



(a)



(b)

Fig. 22: Computation costs of the MILP problems for the cable–strut structure. “◀” and “▶” correspond to the costs for obtaining the upper and lower bounds in Figure 20, respectively. (a) Computation time; and (b) number of enumeration nodes explored by the MILP solver.

- putational Mechanics*, **60**, 813–826 (2017).
16. IBM ILOG: *IBM ILOG CPLEX Optimization Studio*. <https://www.ibm.com/products/ilog-cplex-optimization-studio/> (Accessed November 2023).
 17. M. Ito, N. H. Kim, N. Kogiso: Conservative reliability index for epistemic uncertainty in reliability-based design optimization. *Structural and Multidisciplinary Optimization*, **57**, 1919–1935 (2018).
 18. Y. Jung, H. Cho, Z. Duan, I. Lee: Determination of sample size for input variables in RBDO through bi-objective confidence-based design optimization under input model uncertainty. *Structural and Multidisciplinary Optimization*, **61**, 253–266 (2020).
 19. Y. Jung, H. Cho, I. Lee: Reliability measure approach for confidence-based design optimization under insufficient input data. *Structural and Multidisciplinary Optimization*, **60**, 1967–1982 (2019).
 20. Y. Kanno: Mixed-integer second-order cone programming for global optimization of compliance of frame structure with discrete design variables. *Structural and Multidisciplinary Optimization*, **54**, 301–316 (2016).
 21. Y. Kanno: A data-driven approach to non-parametric reliability-based design optimization of structures

- with uncertain load. *Structural and Multidisciplinary Optimization*, **60**, 83–97 (2019).
22. Y. Kanno: Mixed-integer programming formulation of a data-driven solver in computational elasticity. *Optimization Letters*, **13**, 1505–1514 (2019).
 23. Y. Kanno: Dimensionality reduction enhances data-driven reliability-based design optimizer. *Journal of Advanced Mechanical Design, Systems, and Manufacturing*, **14**, 19-00200 (2020).
 24. Y. Kanno: On three concepts in robust design optimization: absolute robustness, relative robustness, and less variance. *Structural and Multidisciplinary Optimization*, **62**, 979–1000 (2020).
 25. Y. Kanno: A kernel method for learning constitutive relation in data-driven computational elasticity. *Japan Journal of Industrial and Applied Mathematics*, **38**, 39–77 (2021).
 26. Y. Kanno: Alternating minimization for data-driven computational elasticity from experimental data: kernel method for learning constitutive manifold. *Theoretical and Applied Mechanics Letters*, **11**, 100289 (2021).
 27. Y. Kanno: Computation-with-confidence for static elasticity: data-driven approach with order statistics. *Zeitschrift für Angewandte Mathematik und Mechanik*, **103**, e202100482 (2023).
 28. K. Karapiperis, L. Stainier, M. Ortiz, J. E. Andrade: Data-driven multiscale modeling in mechanics. *Journal of the Mechanics and Physics of Solids*, **147**, 104239 (2021).
 29. T. Kirchdoerfer, M. Ortiz: Data-driven computational mechanics. *Computer Methods in Applied Mechanics and Engineering*, **304**, 81–101 (2016).
 30. J. Kleinberg, E. Tardos: *Algorithm Design*. Pearson Education, Boston (2006).
 31. A. Leygue, M. Coret, J. Réthoré, L. Stainier, E. Verron: Data-based derivation of material response. *Computer Methods in Applied Mechanics and Engineering*, **331**, 184–196 (2018).
 32. H. Luo, S. G. Paal: A novel outlier-insensitive local support vector machine for robust data-driven forecasting in engineering. *Engineering with Computers*, **39**, 3671–3689 (2023).
 33. M.-Y. Moon, H. Cho, K. K. Choi, N. Gaul, D. Lamb, D. Gorsich: Confidence-based reliability assessment considering limited numbers of both input and output test data. *Structural and Multidisciplinary Optimization*, **57**, 2027–2043 (2018).
 34. J. Mora-Macías, J. Ayensa-Jiménez, E. Reina-Romo, M. H. Doweidar, J. Domínguez, M. Doblaré, J. A. Sanz-Herrera: A multiscale data-driven approach for bone tissue biomechanics. *Computer Methods in Applied Mechanics and Engineering*, **368**, 113136, (2020).
 35. L. T. K. Nguyen, M.-A. Keip: A data-driven approach to nonlinear elasticity. *Computers and Structures*, **194**, 97–115 (2018).
 36. L. T. K. Nguyen, M. Rambausek, M.-A. Keip: Variational framework for distance-minimizing method in data-driven computational mechanics. *Computer Methods in Applied Mechanics and Engineering*, **365**, 112898 (2020).
 37. D. K. N. Pham, N. Blal, A. Gravouil: Tangent space data driven framework for elasto-plastic material behaviors. *Finite Elements in Analysis and Design*, **216**, 103895 (2023).
 38. K. Poelstra, T. Bartel, B. Schweizer: A data-driven framework for evolutionary problems in solid mechanics. *Zeitschrift für Angewandte Mathematik und Mechanik*, **103**, e202100538 (2023).
 39. E. Prume, S. Reese, M. Ortiz: Model-free data-driven inference in computational mechanics. *Computer Methods in Applied Mechanics and Engineering*, **403**, 115704 (2023).
 40. L. Stainier, A. Leygue, M. Ortiz: Model-free data-driven methods in mechanics: material data identification and solvers. *Computational Mechanics*, **64**, 381–393 (2019).
 41. T.-H. Su, J. G. Jean, C.-S. Chen: Model-free data-driven identification algorithm enhanced by local manifold learning. *Computational Mechanics volume*, **71**, 637–655 (2023).
 42. S. Tang, Y. Li, H. Qiu, H. Yang, S. Saha, S. Mojmuder, W. K. Liu, X. Guo: MAP123-EP: A mechanistic-based data-driven approach for numerical elastoplastic analysis. *Computer Methods in Applied Mechanics and Engineering*, **364**, 112955 (2020).
 43. S. Tang, H. Yang, H. Qiu, M. Fleming, W. K. Liu, X. Guo: MAP123-EPF: A mechanistic-based data-driven approach for numerical elastoplastic modeling at finite strain. *Computer Methods in Applied Mechanics and Engineering*, **373**, 113484 (2021).
 44. S. Tang, G. Zhang, H. Yang, Y. Li, W. K. Liu, X. Guo: MAP123: a data-driven approach to use 1D data for 3D nonlinear elastic materials modeling. *Computer Methods in Applied Mechanics and Engineering*, **357**, 112587 (2019).
 45. İ. Temizer, P. Wriggers: An adaptive method for homogenization in orthotropic nonlinear elasticity. *Computer Methods in Applied Mechanics and Engineering*, **196**, 3409–3423 (2007).
 46. K. Terada, J. Kato, N. Hirayama, T. Inugai, K. Yamamoto: A method of two-scale analysis with micro-macro decoupling scheme: application to hyperelastic composite materials. *Computational Mechanics*, **52**, 1199–1219 (2013).

47. Y. Wang, P. Hao, H. Yang, B. Wang, Q. Gao: A confidence-based reliability optimization with single loop strategy and second-order reliability method. *Computer Methods in Applied Mechanics and Engineering*, **372**, 113436 (2020).
48. I. Watanabe, K. Terada: A method of predicting macroscopic yield strength of polycrystalline metals subjected to plastic forming by micro-macro de-coupling scheme. *International Journal of Mechanical Sciences*, **52**, 343–355 (2010).
49. R. Xu, J. Yang, W. Yan, Q. Huang, G. Giunta, S. Belouettar, H. Zahrouni, T. Ben Zineb, H. Hu: Data-driven multiscale finite element method: from concurrence to separation, *Computer Methods in Applied Mechanics and Engineering*, **363**, 112893 (2020).